© 2017. Published by The Company of Biologists Ltd | Journal of Cell Science (2017) 130, 2673-2681 doi:10.1242/jcs.201012

SHORT REPORT

Re-examining the role of Cdc14 phosphatase in reversal of Cdk phosphorylation during mitotic exit

Brendan L. Powers and Mark C. Hall*

ABSTRACT

Inactivation of cyclin-dependent kinase (Cdk) and reversal of Cdk phosphorylation are universally required for mitotic exit. In budding yeast (*Saccharomyces cerevisiae*), Cdc14 is essential for both and thought to be the major Cdk-counteracting phosphatase. However, Cdc14 is not required for mitotic exit in many eukaryotes, despite highly conserved biochemical properties. The question of how similar enzymes could have such disparate influences on mitotic exit prompted us to re-examine the contribution of budding yeast Cdc14. By using an auxin-inducible degron, we show that severe Cdc14 depletion has no effect on the kinetics of mitotic exit and bulk Cdk substrate dephosphorylation, but causes a cell separation defect and is ultimately lethal. Phosphoproteomic analysis revealed that Cdc14 is highly selective for distinct Cdk sites *in vivo* and does not catalyze widespread Cdk substrate dephosphorylation. We conclude that additional phosphatases likely contribute substantially to Cdk substrate dephosphorylation and coordination of mitotic exit in budding yeast, similar to in other eukaryotes, and the critical mitotic exit functions of Cdc14 require trace amounts of enzyme. We propose that Cdc14 plays very specific, and often different, roles in counteracting Cdk phosphorylation in all species.

KEY WORDS: Cdc14, Protein phosphatase, Mitotic exit, Mitosis, Cyclin-dependent kinase, Cytokinesis

INTRODUCTION

Eukaryotic cell division depends on periodic cyclin-dependent kinase (Cdk) activity (Nigg, 1995). Whereas Cdk activity drives cell cycle events through metaphase, inactivation of Cdk and dephosphorylation of Cdk substrates are required for mitotic exit (Skoufias et al., 2007; Bouchoux and Uhlmann, 2011). Early studies in budding yeast (*Saccharomyces cerevisiae*) revealed that the Cdc14 phosphatase is essential for mitotic exit; cells with temperature-sensitive *cdc14* alleles (Hartwell et al., 1973) arrest after anaphase with high Cdk activity at the restrictive temperature (Visintin et al., 1998). Biochemical and structural evidence suggested that Cdc14 enzymes selectively target Cdk phosphorylation sites (Gray et al., 2003; Visintin et al., 1998; Kaiser et al., 2002). These observations led to the oft-cited model that Cdc14 both terminates Cdk activity and provides the major phosphatase activity for reversing Cdk phosphorylation during mitotic exit (Stegmeier and Amon, 2004).

Department of Biochemistry and Center for Cancer Research, Purdue University, West Lafayette, IN 47907, USA.

*Author for correspondence (mchall@purdue.edu)

M.C.H., 0000-0001-6429-2506

Received 23 December 2016; Accepted 26 June 2017

However, Cdc14 orthologs in other systems are not required for Cdk substrate dephosphorylation and mitotic exit (Mocciaro and Schiebel, 2010; Clemente-Blanco et al., 2006; Wei et al., 2011; Mocciaro et al., 2010; Cueille et al., 2001; Trautmann et al., 2001; Saito et al., 2004; Berdougo et al., 2008). Instead, critical roles for the PP1 and PP2A phosphatases in reversing mitotic Cdk phosphorylation have been reported (Mochida et al., 2009; Wu et al., 2009; Wurzenberger and Gerlich, 2011; Grallert et al., 2015). This suggested that Cdc14 is functionally divergent across species. Nevertheless, human Cdc14B complements the essential Cdc14 function in budding yeast (Vazquez-Novelle et al., 2005) and the activity and specificity of Cdc14 orthologs are highly conserved (Bremmer et al., 2012; Eissler et al., 2014; Li et al., 2015). All Cdc14 enzymes examined exhibit strong selectivity for the pSer-Pro-x-Lys>Arg sub-class of Cdk sites *in vitro* (where pSer is phosphoserine, x is any amino acid and Lys is preferred over Arg), arguing against Cdc14 being a general Cdk-opposing phosphatase *in vivo*. This prompted us to re-evaluate the model that Cdc14 is the major Cdk-counteracting phosphatase during mitotic exit in budding yeast.

RESULTS AND DISCUSSION

Cdc14-depleted cells do not exhibit mitotic exit arrest

In current budding yeast cell cycle models, mitotic exit depends on the Cdc14:Cdk activity ratio. Distinct events are thought to be triggered at different ratios, creating order during mitotic exit (Bouchoux and Uhlmann, 2011). Mathematical models based on empirical data and supported by mutant phenotypes (Kraikivski et al., 2015) reflect the dependence of mitotic exit on Cdc14 concentration. One model, in which a critical Cdc14:Cdk threshold is the trigger for mitotic exit (Drapkin et al., 2009), predicts cell cycle arrest upon lowering Cdc14 below 50% of its normal level (Fig. S1A) and another model predicts the same when it is below 15% (Kraikivski et al., 2015) (Fig. 1A). Interestingly, in recent studies using inducible degrons to deplete Cdc14, the mitotic exit arrest of classical temperature-sensitive *cdc14* alleles was not observed (Jungbluth et al., 2010; Taxis et al., 2009). To quantitatively measure the effect of Cdc14 depletion on mitotic exit kinetics, we engineered a strain expressing Cdc14 with a C-terminal V5 epitope and auxin-inducible degron (AID) tag (Nishimura et al., 2009).

In the absence of auxin, the growth rate and kinetics of a single cell-division cycle were indistinguishable between *CDC14–AID* and wild-type cultures (Fig. S1B,C). Consistent with the essential Cdc14 function, *CDC14–AID* cells failed to grow on agar medium containing the auxin 3-indoleacetic acid (IAA; Fig. 1B). The AID tag alone resulted in ∼70% reduction in the Cdc14 level in liquid cultures, even without IAA addition (Fig. 1C). Addition of IAA consistently depleted 97% of the Cdc14–AID protein, resulting in a combined reduction to 1% of normal Cdc14 concentration (Fig. 1D). Surprisingly, *CDC14–AID* cultures continued to grow

Journal of Cell Science (2017) 130, 2673-2681 doi:10.1242/jcs.201012

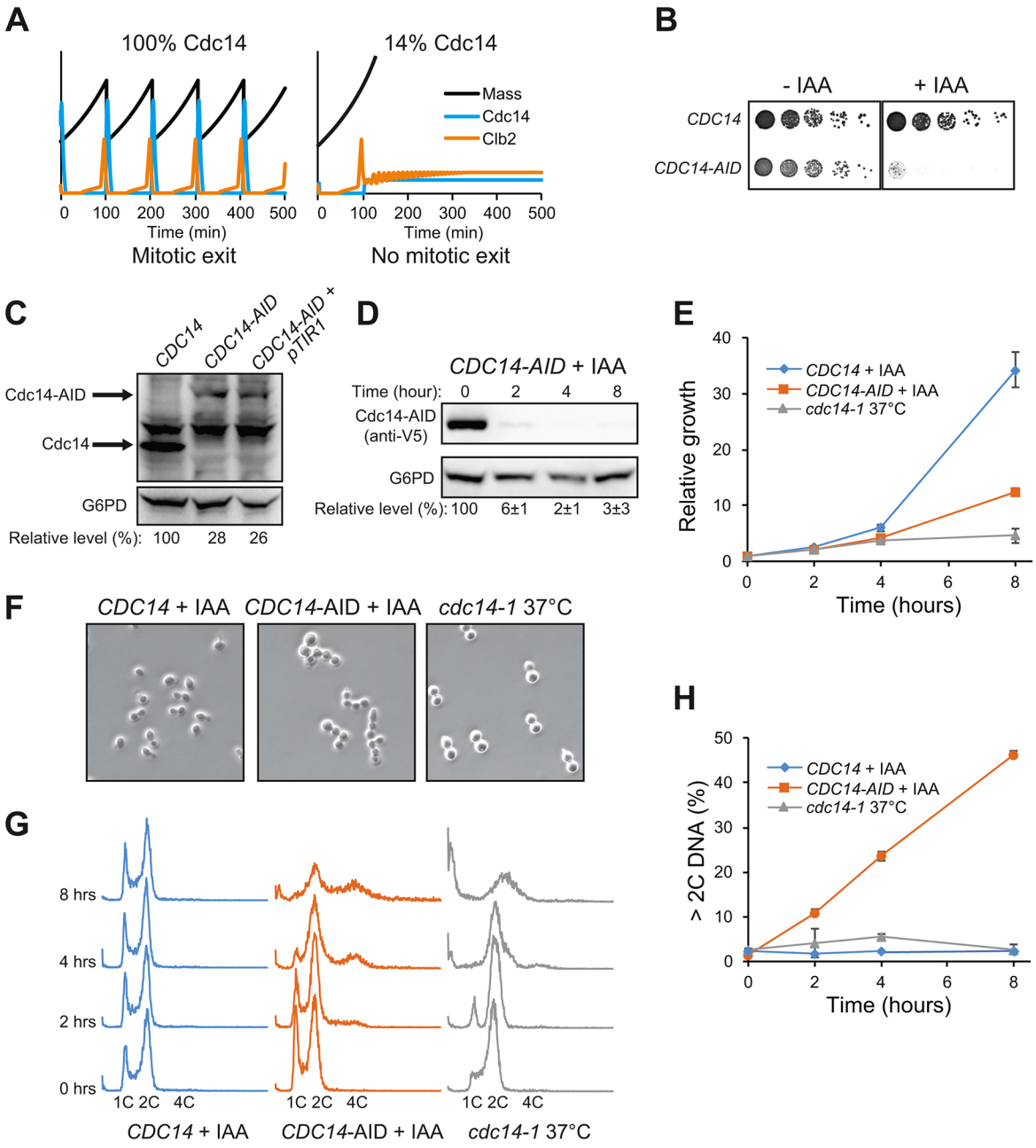

Fig. 1. Cdc14-depleted cells do not arrest at mitotic exit. (A) Computational cell cycle model (Kraikivski et al., 2015) showing predicted impact on mitotic exit of reducing Cdc14 level below 15%. Black, cell mass; orange, Clb2 level; cyan, Cdc14 activity. (B) Serial dilutions of *CDC14* and *CDC14–AID* strains were spotted and grown on YPD plates with and without 250 µM IAA. (C) Cdc14 and Cdc14–AID levels were compared by immunoblotting using anti-Cdc14 antibody. (D) Cdc14–AID was monitored over time by anti-V5 immunoblotting after addition of 250 µM IAA. In C and D, relative Cdc14 signals were adjusted based on G6PD loading control and reported as percentages relative to untagged Cdc14 (C) or time 0 (D). (E) Relative growth of the indicated strains after 250 µM IAA addition (*CDC14* and *CDC14–AID*) or shift to 37°C (*cdc14-1*) based on OD_{600}. (F) Phase-contrast microscopy of cultures from panel E at 8 h. (G) DNA content of cultures from panel E analyzed by flow cytometry. (H) The fraction of cells with >2C DNA content from panel G was quantified and plotted as a function of time. Results for *CDC14* and *CDC14–AID* with IAA treatment were similar at 37°C (data not shown). Data in E and H are mean±s.d., *n*=3.

after IAA treatment, albeit at a reduced rate compared to those for wild-type cultures (Fig. 1E), and failed to exhibit the characteristic mitotic exit arrest morphology of *cdc14-1* cells at 37°C (large-budded 'dumbbells'), even after 8 h (Fig. 1F). Instead, they exhibited a pronounced cell separation defect, forming connected chains and displaying increased DNA content (Fig. 1G,H) consistent with reported functions for Cdc14 in regulating cytokinesis and septation (Kuilman et al., 2015; Chin et al., 2012; Palani et al., 2012; Miller et al., 2015; Bembenek et al., 2005). Mitotic exit in Cdc14–AID-depleted cells was still dependent on the mitotic exit network. A *cdc15-2 CDC14–AID* strain uniformly arrested in late mitosis at 37°C in the presence of IAA (Fig. S1D), ruling out the possibility that lower Cdc14 circumvents normal mitotic exit controls.

Specific activity (Fig. S1E) and substrate specificity (data not shown) of recombinant GST–Cdc14–AID was comparable to that of wild-type GST–Cdc14, demonstrating that the tag does not perturb enzyme activity. To ensure that Cdc14–AID depletion

resulted in a corresponding decrease in cellular Cdc14 activity, we immunoaffinity-isolated Cdc14–AID from extracts generated before and after IAA treatment (Fig. S1F). In a phosphopeptide assay (Bremmer et al., 2012), we found that the recovered phosphatase activity was phosphoserine-specific and inhibited by the specific Cdc14 inhibitor Net1, confirming we were monitoring Cdc14–AID. Importantly, this activity was proportional to the level of Cdc14–AID protein (Fig. S1F), demonstrating that specific activity is not affected by changes in Cdc14 concentration.

The continued cycling of *CDC14–AID* cells expressing Cdc14 at ∼1% of its normal level and activity is inconsistent with mitotic exit events being strictly dependent on specific Cdc14:Cdk activity ratios.

Cdc14-depleted cells exit mitosis with normal kinetics

To quantitatively examine mitotic exit kinetics after Cdc14 depletion, we synchronized cultures in G1 and released them in the presence or absence of IAA (Fig. 2A,B). The kinetics of proteolysis for the mitotic cyclin Clb2 were indistinguishable in the presence and absence of IAA (Fig. 2A,C), suggesting that mitotic exit occurred with normal timing after severe Cdc14 depletion. Failure to exit mitosis should result in the maintenance of ∼50% of Clb2 protein (Yeong et al., 2000) (Fig. 1A). In addition, the kinetics of bulk chromosome segregation and spindle disassembly were indistinguishable in the two cultures (Fig. 2D,E; Fig. S2A). Since Clb2 proteolysis, spindle disassembly and chromosome segregation all depend, to some extent, on dephosphorylation of Cdk substrates (Mocciaro and Schiebel, 2010; Sullivan and Morgan, 2007), these results question the idea that Cdc14 is the major Cdk-opposing phosphatase during mitotic exit. Furthermore, the kinetics of Cdk substrate dephosphorylation were similar in Cdc14-depleted cells, based on immunoblotting for consensus Cdk phospho-site epitopes (Fig. 2F,G). Even the known Cdc14 substrate Acm1 was still dephosphorylated with similar kinetics in Cdc14-depleted cells (Fig. S2B,C). Despite the normal mitotic exit kinetics, the synchronized Cdc14-depleted cells clearly exhibited a separation defect based on microscopy and flow cytometry analyses (Fig. 2E,H; Fig. S2D,E). Again, these results suggest that normal Cdc14 concentration is important for cytokinesis and/or septation, but not for Cdk inactivation and mitotic exit.

Cdc14 is not a general Cdk-counteracting phosphatase *in vivo*

The conserved specificity of Cdc14 enzymes for pSer-Pro-x-Lys>Arg Cdk sites defined using *in vitro* assays has only been validated *in vivo* with a couple of substrates (Bremmer et al., 2012; Eissler et al., 2014). It is partially supported by recent phosphoproteomic studies (Kuilman et al., 2015; Kao et al., 2014), albeit ones not designed to directly assess Cdc14 specificity. We designed a phosphoproteomic experiment to define the *in vivo* substrate specificity of Cdc14 and test whether it generally dephosphorylates Cdk-type sites (Fig. 3A). We arrested control and *pGAL1-CDC14-3MYC* cultures in metaphase with nocodazole to maximize Cdk phosphorylation, added galactose to both (inducing Cdc14 overexpression in *pGAL1-CDC14-3MYC* cells) and harvested aliquots at regular intervals. Since Cdc14 overexpression eventually causes Cdk inactivation through *SIC1* expression and cyclin proteolysis (Visintin et al., 1998), we monitored Clb2 by immunoblotting as an indicator of Cdk inactivation. After Cdk inactivation, dephosphorylation of Cdk sites is less likely to reflect direct Cdc14 action. Cdc14–3Myc protein and activity appeared 30–45 min after galactose addition, based on immunoblotting for Cdc14–3Myc and the early Cdc14 substrate Ask1 (Bouchoux and Uhlmann, 2011) (Fig. 3B). Clb2 degradation to mitotic exit levels occurred after 60 min.

A label-free mass spectrometry workflow (Gillet et al., 2012) was used to identify (Fig. 3C) and quantify (Fig. 3D–F) phosphopeptides across all time points. After extensive filtering to ensure that high-quality spectra and unambiguously identified phosphorylation sites were being used, normalized decay profiles were generated for each site (Fig. 3G). Profiles were subjected to soft clustering to identify groups with similar dephosphorylation kinetics (Fig. S3). The majority of phosphopeptides were stable in both control and Cdc14-induced samples (Fig. 4A; Fig. S3; Table S1). Only 6% of phosphopeptide signals decayed specifically in the Cdc14-induced culture with a half-life of less than the 60-min limit we imposed based on Clb2 degradation (Fig. 4B; Table S1). This group of proteins with rapidly dephosphorylated sites displayed an enrichment for known Cdc14 substrates (some substrates were not represented in our phosphopeptide collection presumably due to low expression), Cdc14-interacting proteins and proteins involved in Cdc14-mediated biological processes (Fig. 4C,D; Table S2). Only 18% of the pSer/pThr-Pro Cdk-type sites were in the rapidly dephosphorylated class (Fig. 4E), and many remained stable throughout the entire time course. Some of these sites could be deposited by other proline-directed kinases. However, if we conservatively consider only Cdk-type sites from known Cdk substrates as identified in two prior large-scale studies (Holt et al., 2009; Ubersax et al., 2003), we still find only 22% are in the rapidly dephosphorylated class (Table S1). The dephosphorylated sites were dramatically enriched for the *in vitro*-defined optimal Cdc14 motif Ser-Pro-x-Lys>Arg (Fig. 4F,G), suggesting that *in vivo* Cdc14 specificity is the same. In fact, the majority of quantified pSer-Pro-x-Lys sites were rapidly dephosphorylated (Fig. 4G). pThr-Pro Cdk sites and non-Cdk sites were poorly represented in the dephosphorylated class.

We conclude that Cdc14 is not a general Cdk-opposing phosphatase in budding yeast as is commonly reported. This conclusion is consistent with a study that monitored dephosphorylation of selected Cdk substrates in the presence and absence of active Cdc14 following Cdk inhibition (Bloom and Cross, 2007). Our observations of unperturbed mitotic exit and Cdk substrate dephosphorylation kinetics upon severe Cdc14 depletion raise the possibility that other phosphatases contribute to bulk Cdk site dephosphorylation, similar to what is observed in other species. It will be important in the future to determine whether PP1 and PP2A enzymes perform this function as they do in fission yeast and vertebrates (Mochida et al., 2009; Wu et al., 2009; Schmitz et al., 2010; Grallert et al., 2015), which would suggest that phosphatase regulation of mitotic exit is broadly conserved across eukaryotes.

Cdc14 has been implicated in determining the order of Cdk substrate dephosphorylation during mitotic exit (Bouchoux and Uhlmann, 2011), although the mechanism is not known. Our phosphoproteomic results support this idea, suggesting that the intrinsic specificity of Cdc14 can contribute to providing an order of Cdk substrate dephosphorylation. Cdc14 likely has the ability to selectively dephosphorylate its optimal substrate motif at times (e.g. early anaphase in budding yeast) when overall Cdk activity is high (Tomson et al., 2009; Geil et al., 2008). The importance of this specificity is reflected in its strict conservation across the fungal and animal kingdoms (Bremmer et al., 2012; Eissler et al., 2014; Li et al., 2015).

Journal of Cell Science (2017) 130, 2673-2681 doi:10.1242/jcs.201012

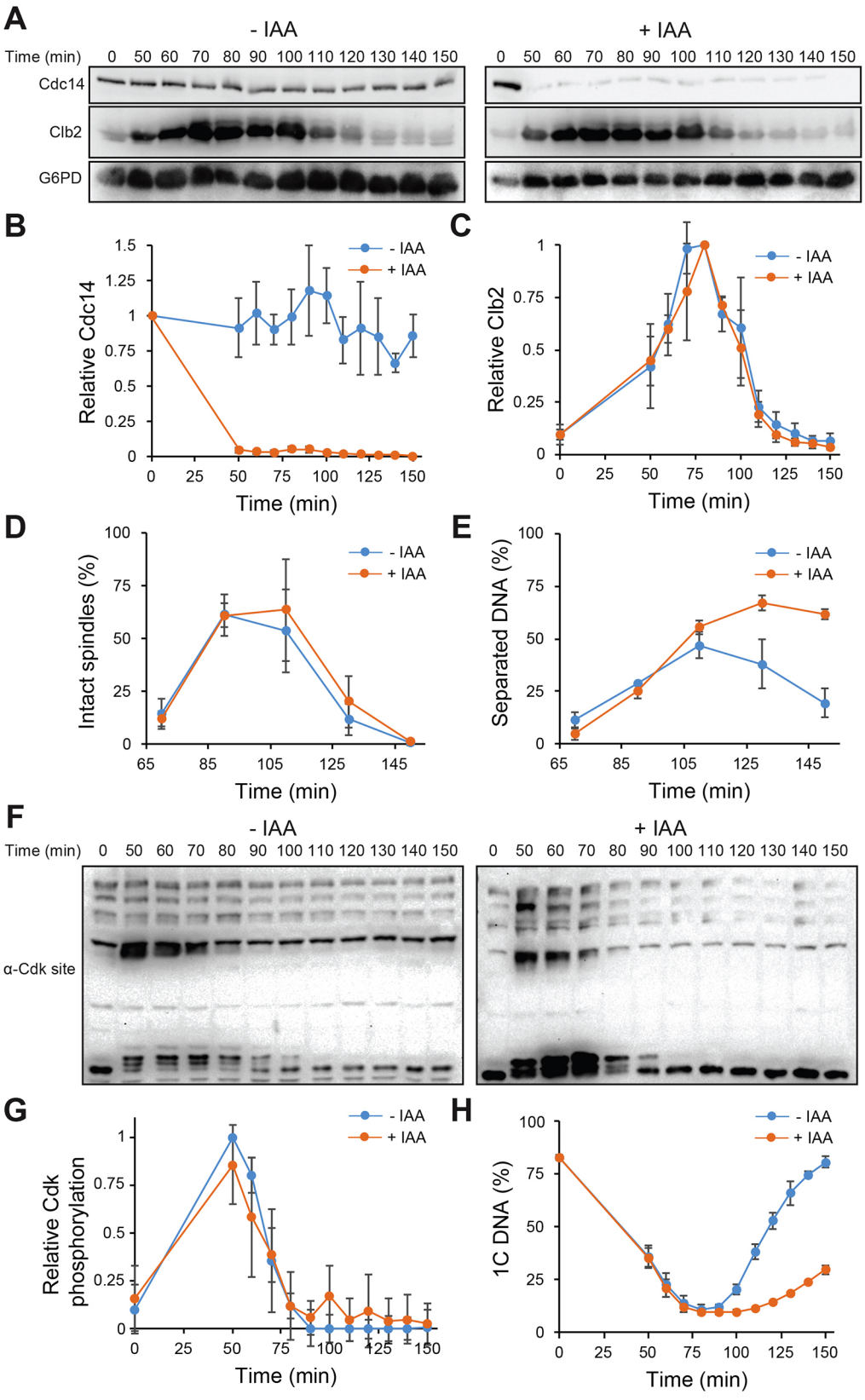

Fig. 2. Cdc14-depleted cells have normal mitotic exit kinetics. *CDC14–AID* culture was synchronized in G1 with α-factor and released with or without 250 µM IAA. After 60 min, α-factor was added again. (A) Cdc14–AID and Clb2 were monitored by anti-V5 and anti-Clb2 immunoblotting. G6PD is a loading control. (B) Cdc14–AID signals were adjusted based on G6PD and normalized to values at time 0. (C) Clb2 signals were adjusted based on G6PD and normalized to the values at the peak level. (D) The fraction of cells with intact spindles was determined by fluorescence microscopy detection of Tub1–GFP (Fig. S2A). (E) The fraction of budded cells with segregated DNA masses was determined by fluorescence microscopy and DAPI staining (Fig. S2A). (F) Global Cdk phosphorylation was monitored by immunoblotting for the Cdk phosphosite epitopes Pro-x-pSer-Pro and pSer-Pro-x-Arg/Lys in whole-cell extracts. (G) Total lane signals from panel F were quantified, the G1 signal at the end of the experiment subtracted from each, and results were normalized to the maximum intensity. (H) DNA content was measured by flow cytometry and the fraction of cells with 1C DNA was quantified and plotted over time. All graphs show averages of three biological replicates as mean±s.d.

The essential requirement for *CDC14* in *Saccharomyces cerevisiae* likely reflects a unique function that evolved in this lineage in terminating Cdk activity via dephosphorylation of a few substrates, possibly Cdh1, which is required for cyclin proteolysis, and Swi5, which is required for expression of the Cdk inhibitor Sic1 (Visintin et al., 1998). However, *cdh1Δ sic1Δ* cells exit mitosis, despite being inviable, implying the existence of at least one other essential mitotic exit Cdc14 substrate (Wasch and Cross, 2002). The

Journal of Cell Science (2017) 130, 2673-2681 doi:10.1242/jcs.201012

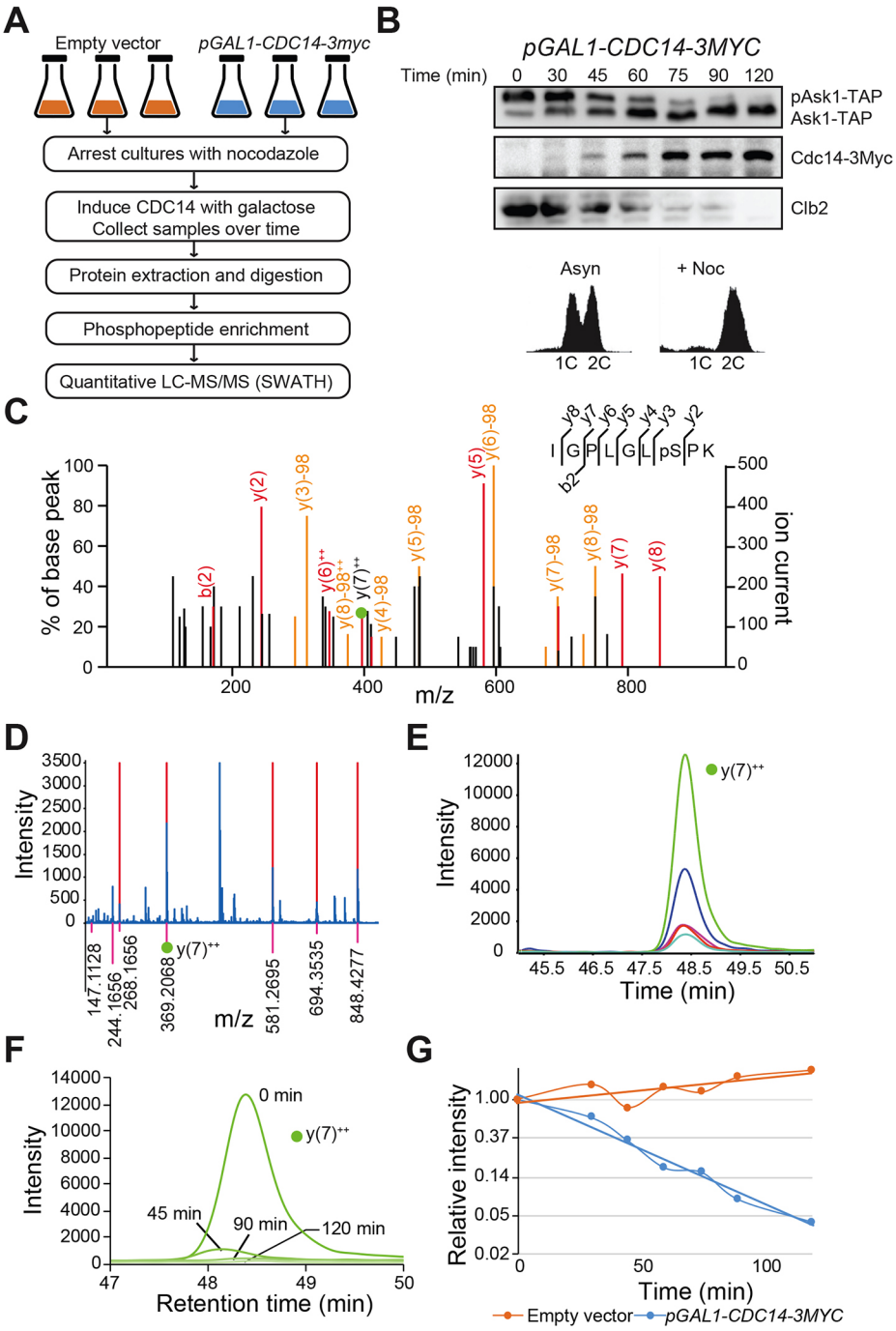

Fig. 3. Phosphoproteomic workflow. (A) Experimental overview. (B) Levels of phosphorylated Ask1–TAP (pAsk1–TAP), Cdc14–3Myc and Clb2 were monitored by immunoblotting after galactose induction in *pGAL1-CDC14-3MYC* cells (top). Nocodazole (+Noc) arrest after 2 h was confirmed by flow cytometry (bottom). Asyn, asynchronous. (C) Spectral library construction for SWATH-MS involves data-dependent LC-MS/MS identification of phosphopeptides such as IGPLGLpSPK (pS is phosphoserine) from Rpl12B. (D) Example data-independent acquisition of fragment spectra from incremental *m*/*z* windows acquired during the LC run (SWATH). The SWATH window for 499 to 525 *m*/*z* is shown. Pink lines below *x*-axis are fragments from the phosphopeptide in C. Fragments used for quantification are indicated in red. (E) Phosphopeptide *m*/*z*, retention time and selected fragment ion *m*/*z* were used to extract quantitative abundance profiles from the SWATH data (each color represents a different red fragment from D). (F) Extracted SWATH signal for a single fragment (*m*/*z* 369.207; green ball in C–E) at different times showing signal loss with dephosphorylation. (G) Integrated SWATH signals from F (three biological replicates) are normalized, averaged, natural log-transformed, and plotted to generate decay profiles. The final profile for phosphopeptide in panel C is shown (blue, *pGAL1-CDC14-3MYC* sample; orange, negative control). Half-lives are determined from linear regression. Proteomics data were deposited to the ProteomeXchange Consortium via the PRIDE partner repository with dataset identifier PXD005237.

essential Cdc14 function likely involves positive feedback that makes mitotic exit switch-like (Lopez-Aviles et al., 2009; Novak et al., 2007), and it seems reasonable that a small fraction of the normal Cdc14 activity could be sufficient to trigger such feedback circuits. The consequent decline in Cdk activity could then allow other phosphatase activities to catalyze the majority of Cdk substrate dephosphorylation. Another plausible (and not mutually exclusive) explanation for the essential function of Cdc14 is that it is needed to directly trigger activation of one or more other phosphatases that drive the majority of the Cdk substrate dephosphorylation required for mitotic exit.

Our results revealed that normal Cdc14 abundance is important for proper cell separation. Cdc14 localizes to the bud neck during cytokinesis and has several recently identified substrates and functions involved in cytokinesis and septation (Kuilman et al., 2015; Chin et al., 2012; Palani et al., 2012; Miller et al., 2015; Mancini Lombardi et al., 2013; Sanchez-Diaz et al., 2012). The significance of Cdc14 localization to the division site following Cdk inactivation remains unclear. Inhibitory Cdk sites there could be inaccessible to other phosphatases or Cdk activity could persist longer there. Cdc14 has been linked to cytokinesis in several other organisms (Li et al., 2015; Wang et al., 2013; Huang et al., 2014; Kaiser et al., 2002, 2004; Mailand et al., 2002; Gruneberg et al., 2002; Au Yong et al., 2016), including *Schizosaccharomyces pombe*, where the Cdc14 ortholog, Clp1, helps coordinate cytokinesis with the nuclear division cycle (Trautmann et al.,

Journal of Cell Science (2017) 130, 2673-2681 doi:10.1242/jcs.201012

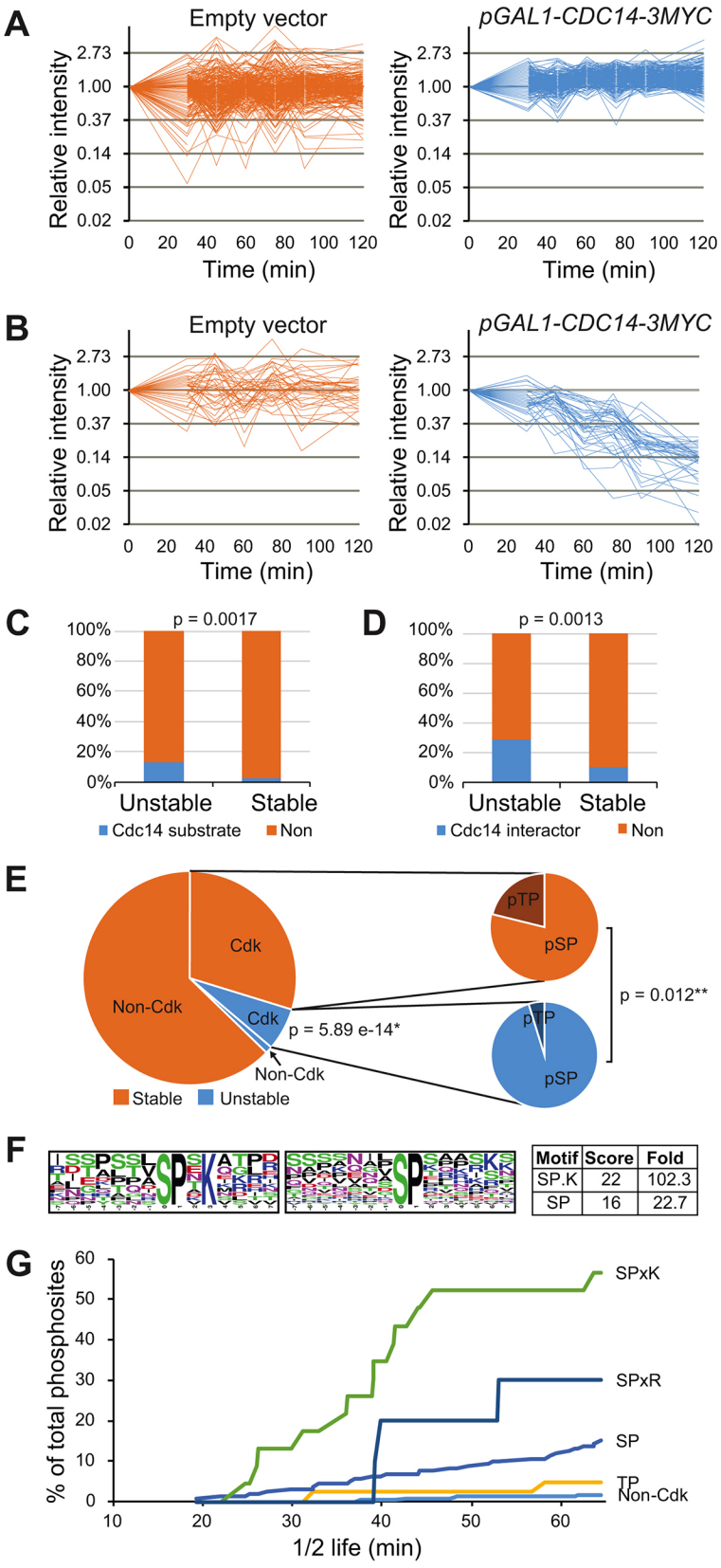

Fig. 4. Cdc14 exhibits specificity for distinct Cdk-type phosphorylation sites *in vivo*. (A,B) Temporal SWATH phosphopeptide profiles after normalization, filtering and clustering; *y*-axes are a natural log scale. (A) Comparison of stable phosphopeptides profiles in cluster 5 (Fig. S3) between samples overexpressing Cdc14–3Myc (right) and empty vector control samples (left). (B) Similar comparison of dephosphorylated peptides in cluster 7 (Fig. S3). (C) Rapidly dephosphorylated proteins were compared to known Cdc14 substrates. The *P*-value from analysis of the fraction of known Cdc14 substrates in the dephosphorylated and stable phosphopeptide sets by a χ-squared test. (D) Same as panel C, with known Cdc14-interacting proteins derived from BioGRID (Chatr-Aryamontri et al., 2015). (E) Phosphosite analysis comparing rapidly dephosphorylated to stable phosphosites. Differences in the fractions of unstable Cdk-type (pSer/pThr-Pro) versus non-Cdk sites (*), and pSer-Pro (pSP) versus pThr-Pro (pTP) sites (**) were analyzed by a χ-squared test. (F) Motif enrichment of rapidly dephosphorylated phosphosites (clusters 3 and 7) with half-lives <60 min. (G) The accumulating fraction of rapidly dephosphorylated sites among the total sites matching each indicated motif.

2001), and promotes proper assembly and function of the contractile ring (Mishra et al., 2004; Clifford et al., 2008). Regulating cytokinesis may represent one of the more broadly conserved Cdc14 functions.

MATERIALS AND METHODS

Yeast strains and plasmids

All yeast strains used in this study are described in Table S3. All yeast plasmid constructs are described in Table S4. Strain YKA1013 was

constructed by integrating a plasmid expressing GFP–TUB1 (pRS306-TUB1) after linearization with StuI. Strain YKA1014 was constructed by integrating a plasmid expressing the *Oryza sativa* Tir1 protein (pAR1103) after linearization with BstEII and PCR-mediated integration of the AID–V5 tag at the 3′ end of the *CDC14* gene (using pAR1070 as template). YKA1034 was created by mating YKA1014 with DLY3034 (a gift from Dr Daniel Lew, Duke University, Durham, NC). The *CDC14–AID* fusion gene was amplified from YKA1014 genomic DNA by PCR and cloned into the Gateway (ThermoFisher Scientific/Invitrogen, Waltham, MA) entry vector pENTR/D-TOPO and transferred from there to the destination vector pDEST15 for *E. coli* expression with an N-terminal GST tag.

Protein purification

GST–Cdc14 and GST–Cdc14–AID were purified on GST-Bind resin (EMD Millipore, Darmstadt, Germany; 70541) at 4°C in 25 mM HEPES-NaOH pH 7.5, 500 mM NaCl, 10% glycerol, 0.1% Triton X-100, 2 mM EDTA, 1 µM pepstatin, 10 µM leupeptin, and 0.5 mM phenylmethylsulfonyl fluoride (PMSF). Proteins were eluted in the same buffer containing 10 mM reduced glutathione, and dialyzed overnight into 25 mM HEPES-NaOH pH 7.5, 300 mM NaCl, 2 mM EDTA, 0.1% β-mercaptoethanol and 40% glycerol. Total protein concentrations were determined with a dye assay (Bio-Rad, Hercules, CA), and the specific concentrations of GST–Cdc14 and GST–Cdc14–AID by digital image analysis of Coomassie Blue-stained SDS-PAGE gels.

Cdc14–AID was isolated from soluble yeast extracts (generated by glass bead lysis) of 500 ml mid-log phase YPD liquid cultures using 100 µl anti-V5 antibody-coupled agarose resin (Sigma-Aldrich, St Louis, MO; A7345) in 40 mM Tris-HCl pH 8.0, 500 mM NaCl, 0.1% Triton X-100, 2 mM EDTA, 10% glycerol, 1 µM pepstatin, 10 µM leupeptin, and 0.5 mM PMSF. The resin was washed 2× with 20 ml of the isolation buffer and then 4× with 1 ml of 25 mM HEPES-NaOH pH 7.5, 100 mM NaCl, 2 mM EDTA and 10 mM sodium fluoride. The resin was then stored at 4°C and used for activity assays within a couple of days.

Phosphatase assays

Activities of recombinant Cdc14 preparations towards 25 mM *p*-nitrophenyl phosphate (pNPP) were measured in 200 µl reactions containing 90 nM enzyme, 25 mM HEPES-NaOH pH 7.5, 0.1% β-mercaptoethanol, 1 mM EDTA and 150 mM NaCl for 30 min at 30°C. When present, activated sodium orthovanadate was included as an inhibitor at 500 µM. Reactions were stopped with 50 µl 5 M NaOH and absorbance measured at 405 nm in a microplate reader. Reaction rates were determined from a standard curve of *p*-nitrophenol measured under identical conditions.

Phosphatase activity associated with anti-V5 resin from Cdc14–AID immunoaffinity isolations towards 200 µM phosphopeptide substrates was measured as described previously (Powers et al., 2016) with the following modifications. 10% of the resin volume was used as the source of enzyme. To stop the reaction, the resin was pelleted and 50 µl was transferred to a microplate well containing 100 µl BIOMOL® green phosphate detection reagent (Enzo Life Sciences, Farmingdale, NY). Reaction rates were calculated using a standard curve generated with sodium phosphate monobasic reagent under identical conditions. The used resin was stripped of protein by boiling in SDS-PAGE dye and subjected to immunoblotting with anti-V5 antibody as described below to determine the relative amount of Cdc14–AID in each reaction.

Asynchronous growth assays

Cultures were grown to log-phase in YPD (20 g/l dextrose, 20 g/l peptone and 10 g/l yeast extract) at 25°C and then diluted to an optical density at 600 nm (OD_{600})=0.300. When required, 3-indoleacetic acid (IAA; Sigma-Aldrich I3750) was added to a final concentration of 250 µM. Cultures were back diluted into pre-warmed YPD to maintain log-phase growth over the entire time course. Samples were collected for flow cytometry, immunoblotting and microscopy over 8 h.

Synchronous cell cycle analysis

Yeast liquid cultures were grown to log-phase in YPD at 30°C, diluted to OD_{600}=0.3 and synchronized in G1 with 5 µg/ml α-factor (synthesized by Genscript, Piscataway, NJ) for 1.5 h. The culture was split and released from G1 by washing with H_2O and resuspending in fresh YPD with or without 250 µM IAA. Cells were re-arrested in the following G1 by adding 5 µg/ml α-factor 60 min after release. Samples were collected for flow cytometry, immunoblotting and microscopy at regular intervals over 150 min.

Immunoblotting

Whole-cell protein extracts were prepared from 5–10 ml cultures for immunoblotting as described previously (Martinez et al., 2006). The following antibodies were used: rabbit anti-protein A (1:10,000; Sigma-Aldrich, P3775), anti-FLAG-M2 monoclonal (1:500; Sigma-Aldrich, F3165), rabbit anti-G6PD (1:5000; Sigma-Aldrich, A9521), anti-c-Myc monoclonal (1:2000; Sigma-Aldrich, 11667149001), rabbit anti-Clb2 (1:2000; Santa Cruz Biotechnology, Santa Cruz, CA, SC9071), rabbit anti-Cdc14 (1:2000; Santa Cruz Biotechnology, SC33628), rabbit antibody against the MAPK/CDK substrate peptides PXpSP or pSPXR/K (1:1000; Cell Signaling Technology, Danvers, MA, 2325), anti-V5 monoclonal conjugated to horseradish peroxidase (HRP) (1:2000; Invitrogen, Carlsbad, CA, R961), rabbit anti-Acm1 (1:10,000; Melesse et al., 2014), and HRP-coupled anti-mouse-IgG or rabbit-IgG secondary antibodies (1:10,000; Jackson ImmunoResearch, West Grove, PA; 115-035-003 or 111-035-003). After exposure to chemiluminescent detection reagent (Luminata Crescendo; EMD Millipore, WBLUR0400), blots were visualized on a ChemiDoc Touch digital imaging system (Bio-Rad) and images analyzed and quantified using ImageLab 5.0 software (Bio-Rad).

Flow cytometry

DNA content of cultures was quantified exactly as described previously (Martinez et al., 2006) by using Sytox Green dye (Molecular Probes, Eugene, OR S7020) on an Accuri C6 flow cytometer (BD Biosciences, San Jose, CA, USA) and either the C6 instrument acquisition software, CFlow Plus or FCS Express (De Novo Software).

DAPI staining and microscopy

Fluorescence and phase-contrast microscopy were performed as described previously (Martinez et al., 2012) using a 60× oil immersion objective on an Olympus BX52 microscope (Olympus, Tokyo, Japan) with an Olympus DP80 digital camera. Quantification of mitotic spindles, DNA segregation, and budding was performed in triplicate with >100 cells counted per sample.

Cdc14 overexpression in arrested cultures

ASK1-TAP cells carrying either an empty vector or a vector overexpressing *CDC14-3MYC* from the *GAL1* promoter were grown in selective raffinose medium (20 g/l raffinose, 6.7 g/l yeast nitrogen base and appropriate amino acid dropout mixture) to log-phase, diluted to OD_{600}=0.3, treated for 2 h with 15 µg/ml nocodazole (Cayman Chemical, Ann Arbor, MI; 13857) for mitotic arrest, and then induced with 2% galactose. 50 ml cell aliquots were harvested at the indicated times, fixed with 6% trichloroacetic acid for 10 min on ice, washed 3× with 10 ml cold acetone and stored at −80°C.

Cell lysis and peptide generation for MS

Soluble protein extracts and tryptic peptide digests were generated under denaturing conditions, and phosphopeptide fractions enriched using TiO_2 resin (Titansphere Phos-TiO; GL Sciences, Tokyo, Japan; 5010-21315) essentially as described previously (Bodenmiller and Aebersold, 2010) with the following minor changes. Cells were lysed using 0.5 mm glass beads and a Disruptor Genie (Cole-Parmer, Vernon Hills, IL) for 10 min at 4°C and clarified by centrifugation at 16,000 ***g*** for 10 min. The insoluble pellet was resuspended and the lysis procedure repeated twice, with the soluble supernatants pooled. 2 mg of protein was reduced with 5 mM dithiothreitol (DTT), alkylated with 15 mM iodoacetamide and quenched with 5 mM DTT. The alkylated proteins were then digested with recombinant trypsin (Trypzean; Sigma-Aldrich T3568) at a 1:100 enzyme:protein ratio for 18 h at 37°C. Sep-Pak Vac 3cc (500 mg) C18 columns (Waters, Milford, MA;

WAT020805) were used to desalt peptides prior to phosphopeptide enrichment.

SWATH mass spectrometry

Dried enriched phosphopeptide samples were resuspended in 20 µl 2% acetonitrile and 0.1% trifluoroacetic acid (TFA) immediately prior to high-pressure liquid chromatography electrospray ionization tandem mass spectrometry (HPLC-ESI-MS/MS) analysis using a NanoLC 400 HPLC system with a cHiPLC-nanoflex module (Eksigent, Dublin, CA, USA) connected to a TripleTOF 5600 mass spectrometer (AB Sciex, Framingham, MA). Peptides were resolved using ChromXP C18-CL trapping (200 µm×0.5 mm) and analytical (75 µm×15 cm) cartridges (3 µm particle size, 120 Å pore size; Eksigent, 5015839 and 804-00001) at a flow rate of 300 nl/min with a 90 min gradient from 5% to 35% acetonitrile in 0.1% TFA (total run time of 120 min). Identical liquid chromatography methods were used for data-dependent acquisition (DDA) and data-independent SWATH acquisition modes. For DDA, the mass spectrometer was operated in positive-ion and high-sensitivity mode with cycles of 250 millisec MS survey scans at between 400 and 1600 *m*/*z* followed by up to 50 MS/MS scans (50 ms each) of the most abundant ions (limited to +2 to +4 charge, intensity >150, 6 s dynamic exclusion at 100 ppm width) using a collision energy (CE) of 10 and a collision energy spread (CES) of 5 (maximum duty cycle=2.75 s). For SWATH acquisition, cycles of a 50 millisecond survey scan covering 400 to 1600 *m*/*z* followed by 50 ms MS/MS fragment ion spectra in incremental 25 *m*/*z* windows from 400 to 1250 *m*/*z* with a 1 *m*/*z* overlap were programmed (total 34 SWATH windows, total cycle time=1.75 s). CE was automatically calculated for each SWATH window and ranged from 22.308 to 73.821 with a CES of 10.

Database searching and SWATH extraction

To prepare a spectral library for SWATH analysis, DDA data from all seven time points were simultaneously submitted to ProteinPilot v 4.5 (AB Sciex) for peptide identification with the following search settings: iodoacetamide cysteine alkylation, trypsin digestion, phosphorylation emphasis, no biological modifications, thorough search effort, *S. cerevisiae* SwissProt database, and false detection rate (FDR) assessed using a reverse decoy database. ProteinPilot search results were imported into Peakview 2.1 (AB Sciex) and filtered to keep only unmodified peptides and peptides with carbamidomethylation, phosphorylation and oxidation modifications. Nine peptides with consistent strong ion signals distributed across the gradient (with retention times from 25 to 85 min) were used within Peakview 2.1 to perform retention time alignment of all SWATH runs. After alignment, SWATH chromatograms for every peptide from the DDA spectral library with ProteinPilot identification confidence >95% were extracted using a 6 min extraction window, *m*/*z* width=50 ppm, and five of the most abundant transitions per peptide.

SWATH data analysis

The extracted SWATH signals were further filtered, normalized (Callister et al., 2006) and analyzed as described in Table S1. The final, high-confidence set of phosphorylation sites was analyzed by soft clustering using fuzzy c-means (FCM) to identify groups with similar temporal decay profiles (Futschik and Carlisle, 2005). For soft clustering, phosphopeptide profiles were required to have <15% missing values, and any missing values were estimated using k-nearest neighbor imputation. FCM was performed with seven centers and an *m* value of 1.25.

Bioinformatic analysis of phosphopeptides

Identification of sequence motifs among the set of rapidly dephosphorylated sites with statistically significant enrichment was performed using Motif-X 1.2 (Chou and Schwartz, 2011). 15-amino-acid windows surrounding the site of phosphorylation were extracted. The sequences were then analyzed using the following parameters: pre-aligned foreground, S or T as the central character, 15-amino-acid widths, minimum of 10 occurrences, $P<0.001$, and a SGD yeast proteome background. Analysis of gene ontology (GO) enrichment was performed using DAVID 6.8 (Huang da et al., 2009). Proteins with rapidly dephosphorylated sites were analyzed by using *Saccharomyces cerevisiae* S288c as the background. Biological processes were clustered using medium stringency: similarity term overlap 3, similarity threshold 0.5, initial group membership 3, final group membership 3, multiple linkage threshold 0.5, and EASE (enrichment threshold) 1.0. GO terms with final *P*-values <0.05 were reported.

Acknowledgements

We thank Adam Rudner, Daniel Lew, and Harry Charbonneau for reagents, and Anton Iliuk, Andy Tao, Yi Yang, Steven Konieczny, Uma Aryal, Vicki Hedrick, John Morgan, and Longyun Guo for technical assistance. We acknowledge support from Purdue University Center for Cancer Research, NIH grant P30 CA023168 for use of shared resources.

Competing interests

The authors declare no competing or financial interests.

Author contributions

Conceptualization: B.L.P., M.C.H.; Methodology: B.L.P., M.C.H.; Formal analysis: B.L.P., M.C.H.; Investigation: B.L.P., M.C.H.; Resources: M.C.H.; Data curation: B.L.P.; Writing - original draft: B.L.P., M.C.H.; Writing - review & editing: B.L.P., M.C.H.; Visualization: B.L.P., M.C.H.; Supervision: M.C.H.; Project administration: M.C.H.; Funding acquisition: M.C.H.

Funding

Purdue University provided funding support.

Data availability

Proteomics data were deposited to the ProteomeXchange Consortium via the PRIDE partner repository with dataset identifier PXD005237.

Supplementary information

Supplementary information available online at
http://jcs.biologists.org/lookup/doi/10.1242/jcs.201012.supplemental

References

Au Yong, J. Y., Wang, Y.-M. and Wang, Y. (2016). The Nim1 kinase Gin4 has distinct domains crucial for septin assembly, phospholipid binding and mitotic exit. *J. Cell Sci.* **129**, 2744-2756.

Bembenek, J., Kang, J., Kurischko, C., Li, B., Raab, J. R., Belanger, K. D., Luca, F. C. and Yu, H. (2005). Crm1-mediated nuclear export of Cdc14 is required for the completion of cytokinesis in budding yeast. *Cell Cycle* **4**, 961-971.

Berdougo, E., Nachury, M. V., Jackson, P. K. and Jallepalli, P. V. (2008). The nucleolar phosphatase Cdc14B is dispensable for chromosome segregation and mitotic exit in human cells. *Cell Cycle* **7**, 1184-1190.

Bloom, J. and Cross, F. R. (2007). Novel role for Cdc14 sequestration: Cdc14 dephosphorylates factors that promote DNA replication. *Mol. Cell. Biol.* **27**, 842-853.

Bodenmiller, B. and Aebersold, R. (2010). Quantitative analysis of protein phosphorylation on a system-wide scale by mass spectrometry-based proteomics. *Methods in Enzymology* **470**, 317-334. Epub 2010 Mar 1.

Bouchoux, C. and Uhlmann, F. (2011). A quantitative model for ordered Cdk substrate dephosphorylation during mitotic exit. *Cell* **147**, 803-814.

Bremmer, S. C., Hall, H., Martinez, J. S., Eissler, C. L., Hinrichsen, T. H., Rossie, S., Parker, L. L., Hall, M. C. and Charbonneau, H. (2012). Cdc14 phosphatases preferentially dephosphorylate a subset of cyclin-dependent kinase (Cdk) sites containing phosphoserine. *J. Biol. Chem.* **287**, 1662-1669.

Callister, S. J., Barry, R. C., Adkins, J. N. Johnson, E. T., Qian, W. J., Webb-Robertson, B. J., Smith, R. D. and Lipton, M. S. (2006). Normalization approaches for removing systematic biases associated with mass spectrometry and label-free proteomics. *J Proteome Res.* **5**, 277-286.

Chatr-Aryamontri, A., Breitkreutz, B.-J., Oughtred, R., Boucher, L., Heinicke, S., Chen, D., Stark, C., Breitkreutz, A., Kolas, N., O'donnell, L. et al. (2015). The BioGRID interaction database: 2015 update. *Nucleic Acids Res.* **43**, D470-D478.

Chin, C. F., Bennett, A. M., Ma, W. K., Hall, M. C. and Yeong, F. M. (2012). Dependence of Chs2 ER export on dephosphorylation by cytoplasmic Cdc14 ensures that septum formation follows mitosis. *Mol. Biol. Cell* **23**, 45-58.

Chou, M. F. and Schwartz, D. (2011). Biological sequence motif discovery using motif-x. *Curr. Protoc. Bioinformatics* Chapter 13, Unit 13 15-24.

Clemente-Blanco, A., González-Novo, A., Machin, F., Caballero-Lima, D., Aragon, L., Sánchez, M., de Aldana, C. R., Jimenez, J. and Correa-Bordes, J. (2006). The Cdc14p phosphatase affects late cell-cycle events and morphogenesis in Candida albicans. *J. Cell Sci.* **119**, 1130-1143.

Clifford, D. M., Wolfe, B. A., Roberts-Galbraith, R. H., Mcdonald, W. H., Yates, J. R., III and Gould, K. L. (2008). The Clp1/Cdc14 phosphatase contributes to the robustness of cytokinesis by association with anillin-related Mid1. *J. Cell Biol.* **181**, 79-88.

Cueille, N., Salimova, E., Esteban, V., Blanco, M., Moreno, S., Bueno, A. and Simanis, V. (2001). Flp1, a fission yeast orthologue of the S. cerevisiae CDC14 gene, is not required for cyclin degradation or Rum1p stabilisation at the end of mitosis. *J. Cell Sci.* **114**, 2649-2664.
Drapkin, B. J., Lu, Y., Procko, A. L., Timney, B. L. and Cross, F. R. (2009). Analysis of the mitotic exit control system using locked levels of stable mitotic cyclin. *Mol. Syst. Biol.* **5**, 328.
Eissler, C. L., Mazón, G., Powers, B. L., Savinov, S. N., Symington, L. S. and Hall, M. C. (2014). The Cdk/Cdc14 module controls activation of the Yen1 holliday junction resolvase to promote genome stability. *Mol. Cell* **54**, 80-93.
Futschik, M. E. and Carlisle, B. (2005). Noise-robust soft clustering of gene expression time-course data. *J. Bioinform. Comput. Biol.* **3**, 965-988.
Geil, C., Schwab, M. and Seufert, W. (2008). A nucleolus-localized activator of Cdc14 phosphatase supports rDNA segregation in yeast mitosis. *Curr. Biol.* **18**, 1001-1005.
Gillet, L. C., Navarro, P., Tate, S., Röst, H., Selevsek, N., Reiter, L., Bonner, R. and Aebersold, R. (2012). Targeted data extraction of the MS/MS spectra generated by data-independent acquisition: a new concept for consistent and accurate proteome analysis. *Mol. Cell. Proteomics* **11**, O111.016717.
Grallert, A., Boke, E., Hagting, A., Hodgson, B., Connolly, Y., Griffiths, J. R., Smith, D. L., Pines, J. and Hagan, I. M. (2015). A PP1-PP2A phosphatase relay controls mitotic progression. *Nature* **517**, 94-98.
Gray, C. H., Good, V. M., Tonks, N. K. and Barford, D. (2003). The structure of the cell cycle protein Cdc14 reveals a proline-directed protein phosphatase. *EMBO J.* **22**, 3524-3535.
Gruneberg, U., Glotzer, M., Gartner, A. and Nigg, E. A. (2002). The CeCDC14 phosphatase is required for cytokinesis in the Caenorhabditis elegans embryo. *J. Cell Biol.* **158**, 901-914.
Hartwell, L. H., Mortimer, R. K., Culotti, J. and Culotti, M. (1973). Genetic control of the cell division cycle in yeast: V. Genetic analysis of cdc mutants. *Genetics* **74**, 267-286.
Holt, L. J., Tuch, B. B., Villen, J., Johnson, A. D., Gygi, S. P. and Morgan, D. O. (2009). Global analysis of Cdk1 substrate phosphorylation sites provides insights into evolution. *Science* **325**, 1682-1686.
Huang, Z.-X., Zhao, P., Zeng, G.-S., Wang, Y.-M., Sudbery, I. and Wang, Y. (2014). Phosphoregulation of Nap1 plays a role in septin ring dynamics and morphogenesis in Candida albicans. *mBio* **5**, e00915-13.
Huang da, W., Sherman, B. T. and Lempicki, R. A. (2009). Systematic and integrative analysis of large gene lists using DAVID bioinformatics resources. *Nat. Protoc.* **4**, 44-57.
Jungbluth, M., Renicke, C. and Taxis, C. (2010). Targeted protein depletion in Saccharomyces cerevisiae by activation of a bidirectional degron. *BMC Syst. Biol.* **4**, 176.
Kaiser, B. K., Zimmerman, Z. A., Charbonneau, H. and Jackson, P. K. (2002). Disruption of centrosome structure, chromosome segregation, and cytokinesis by misexpression of human Cdc14A phosphatase. *Mol. Biol. Cell* **13**, 2289-2300.
Kaiser, B. K., Nachury, M. V., Gardner, B. E. and Jackson, P. K. (2004). Xenopus Cdc14 alpha/beta are localized to the nucleolus and centrosome and are required for embryonic cell division. *BMC Cell Biol.* **5**, 27.
Kao, L., Wang, Y.-T., Chen, Y.-C., Tseng, S.-F., Jhang, J.-C., Chen, Y.-J. and Teng, S.-C. (2014). Global analysis of Cdc14 dephosphorylation sites reveals essential regulatory role in mitosis and cytokinesis. *Mol. Cell. Proteomics* **13**, 594-605.
Kraikivski, P., Chen, K. C., Laomettachit, T., Murali, T. M. and Tyson, J. J. (2015). From START to FINISH: computational analysis of cell cycle control in budding yeast. *Npj Syst. Biol. Appl.* **1**, 15016.
Kuilman, T., Maiolica, A., Godfrey, M., Scheidel, N., Aebersold, R. and Uhlmann, F. (2015). Identification of Cdk targets that control cytokinesis. *EMBO J.* **34**, 81-96.
Li, C., Melesse, M., Zhang, S., Hao, C. F., Wang, C., Zhang, H., Hall, M. C. and Xu, J.-R. (2015). FgCDC14 regulates cytokinesis, morphogenesis, and pathogenesis in Fusarium graminearum. *Mol. Microbiol.* **98**, 770-786.
López-Avilés, S., Kapuy, O., Novak, B. and Uhlmann, F. (2009). Irreversibility of mitotic exit is the consequence of systems-level feedback. *Nature* **459**, 592-595.
Mailand, N., Lukas, C., Kaiser, B. K., Jackson, P. K., Bartek, J. and Lukas, J. (2002). Deregulated human Cdc14A phosphatase disrupts centrosome separation and chromosome segregation. *Nat. Cell Biol.* **4**, 317-322.
Mancini Lombardi, I., Palani, S., Meitinger, F., Darieva, Z., Hofmann, A., Sharrocks, A. D. and Pereira, G. (2013). Lre1 directly inhibits the NDR/Lats kinase Cbk1 at the cell division site in a phosphorylation-dependent manner. *Curr. Biol.* **23**, 1736-1745.
Martinez, J. S., Jeong, D.-E., Choi, E., Billings, B. M. and Hall, M. C. (2006). Acm1 is a negative regulator of the CDH1-dependent anaphase-promoting complex/cyclosome in budding yeast. *Mol. Cell. Biol.* **26**, 9162-9176.
Martinez, J. S., Hall, H., Bartolowits, M. D. and Hall, M. C. (2012). Acm1 contributes to nuclear positioning by inhibiting Cdh1-substrate interactions. *Cell Cycle* **11**, 38-394.
Melesse, M., Choi, E., Hall, H., Walsh, M. J., Geer, M. A. and Hall, M. C. (2014). Timely activation of budding yeast APC^{Cdh1} involves degradation of its inhibitor, Acm1, by an unconventional proteolytic mechanism. *PLoS ONE* **9**, e103517.
Miller, D. P., Hall, H., Chaparian, R., Mara, M., Mueller, A., Hall, M. C. and Shannon, K. B. (2015). Dephosphorylation of Iqg1 by Cdc14 regulates cytokinesis in budding yeast. *Mol. Biol. Cell* **26**, 2913-2926.
Mishra, M., Karagiannis, J., Trautmann, S., Wang, H., Mccollum, D. and Balasubramanian, M. K. (2004). The Clp1p/Flp1p phosphatase ensures completion of cytokinesis in response to minor perturbation of the cell division machinery in Schizosaccharomyces pombe. *J. Cell Sci.* **117**, 3897-3910.
Mocciaro, A. and Schiebel, E. (2010). Cdc14: a highly conserved family of phosphatases with non-conserved functions? *J. Cell Sci.* **123**, 2867-2876.
Mocciaro, A., Berdougo, E., Zeng, K., Black, E., Vagnarelli, P., Earnshaw, W., Gillespie, D., Jallepalli, P. and Schiebel, E. (2010). Vertebrate cells genetically deficient for Cdc14A or Cdc14B retain DNA damage checkpoint proficiency but are impaired in DNA repair. *J. Cell Biol.* **189**, 631-639.
Mochida, S., Ikeo, S., Gannon, J. and Hunt, T. (2009). Regulated activity of PP2A-B55 delta is crucial for controlling entry into and exit from mitosis in Xenopus egg extracts. *EMBO J.* **28**, 2777-2785.
Nigg, E. A. (1995). Cyclin-dependent protein kinases: key regulators of the eukaryotic cell cycle. *BioEssays* **17**, 471-480.
Nishimura, K., Fukagawa, T., Takisawa, H., Kakimoto, T. and Kanemaki, M. (2009). An auxin-based degron system for the rapid depletion of proteins in nonplant cells. *Nat. Methods* **6**, 917-922.
Novak, B., Tyson, J. J., Gyorffy, B. and Csikasz-Nagy, A. (2007). Irreversible cell-cycle transitions are due to systems-level feedback. *Nat. Cell Biol.* **9**, 724-728.
Palani, S., Meitinger, F., Boehm, M. E., Lehmann, W. D. and Pereira, G. (2012). Cdc14-dependent dephosphorylation of Inn1 contributes to Inn1-Cyk3 complex formation. *J. Cell Sci.* **125**, 3091-3096.
Powers, B. L., Melesse, M., Eissler, C. L., Charbonneau, H. and Hall, M. C. (2016). Measuring Activity and Specificity of Protein Phosphatases. *Methods Mol. Biol.* **1342**, 221-235.
Saito, R. M., Perreault, A., Peach, B., Satterlee, J. S. and van den Heuvel, S. (2004). The CDC14 phosphatase controls developmental cell-cycle arrest in C. elegans. *Nat. Cell Biol.* **6**, 777-783.
Sanchez-Diaz, A., Nkosi, P. J., Murray, S. and Labib, K. (2012). The Mitotic Exit Network and Cdc14 phosphatase initiate cytokinesis by counteracting CDK phosphorylations and blocking polarised growth. *EMBO J.* **31**, 3620-3634.
Schmitz, M. H., Held, M., Janssens, V., Hutchins, J. R., Hudecz, O., Ivanova, E., Goris, J., Trinkle-Mulcahy, L., Lamond, A. I., Poser, I. et al. (2010). Live-cell imaging RNAi screen identifies PP2A-B55alpha and importin-beta1 as key mitotic exit regulators in human cells. *Nat. Cell Biol.* **12**, 886-893.
Skoufias, D. A., Indorato, R.-L., Lacroix, F., Panopoulos, A. and Margolis, R. L. (2007). Mitosis persists in the absence of Cdk1 activity when proteolysis or protein phosphatase activity is suppressed. *J. Cell Biol.* **179**, 671-685.
Stegmeier, F. and Amon, A. (2004). Closing mitosis: the functions of the Cdc14 phosphatase and its regulation. *Annu. Rev. Genet.* **38**, 203-232.
Sullivan, M. and Morgan, D. O. (2007). Finishing mitosis, one step at a time. *Nat. Rev. Mol. Cell Biol.* **8**, 894-903.
Taxis, C., Stier, G., Spadaccini, R. and Knop, M. (2009). Efficient protein depletion by genetically controlled deprotection of a dormant N-degron. *Mol. Syst. Biol.* **5**, 267.
Tomson, B. N., Rahal, R., Reiser, V., Monje-Casas, F., Mekhail, K., Moazed, D. and Amon, A. (2009). Regulation of Spo12 phosphorylation and its essential role in the FEAR network. *Curr. Biol.* **19**, 449-460.
Trautmann, S., Wolfe, B. A., Jorgensen, P., Tyers, M., Gould, K. L. and Mccollum, D. (2001). Fission yeast Clp1p phosphatase regulates G2/M transition and coordination of cytokinesis with cell cycle progression. *Curr. Biol.* **11**, 931-940.
Ubersax, J. A., Woodbury, E. L., Quang, P. N., Paraz, M., Blethrow, J. D., Shah, K., Shokat, K. M. and Morgan, D. O. (2003). Targets of the cyclin-dependent kinase Cdk1. *Nature* **425**, 859-864.
Vázquez-Novelle, M. D., Esteban, V., Bueno, A. and Sacristán, M. P. (2005). Functional homology among human and fission yeast Cdc14 phosphatases. *J. Biol. Chem.* **280**, 29144-29150.
Visintin, R., Craig, K., Hwang, E. S., Prinz, S., Tyers, M. and Amon, A. (1998). The phosphatase Cdc14 triggers mitotic exit by reversal of Cdk-dependent phosphorylation. *Mol. Cell* **2**, 709-718.
Wang, J., Liu, J., Hu, Y., Ying, S.-H. and Feng, M.-G. (2013). Cytokinesis-required Cdc14 is a signaling hub of asexual development and multi-stress tolerance in Beauveria bassiana. *Sci. Rep.* **3**, 3086.
Wäsch, R. and Cross, F. R. (2002). APC-dependent proteolysis of the mitotic cyclin Clb2 is essential for mitotic exit. *Nature* **418**, 556-562.
Wei, Z., Peddibhotla, S., Lin, H., Fang, X., Li, M., Rosen, J. M. and Zhang, P. (2011). Early-onset aging and defective DNA damage response in Cdc14B-deficient mice. *Mol. Cell. Biol.* **31**, 1470-1477.
Wu, J. Q., Guo, J. Y., Tang, W., Yang, C.-S., Freel, C. D., Chen, C., Nairn, A. C. and Kornbluth, S. (2009). PP1-mediated dephosphorylation of phosphoproteins at mitotic exit is controlled by inhibitor-1 and PP1 phosphorylation. *Nat. Cell Biol.* **11**, 644-651.
Wurzenberger, C. and Gerlich, D. W. (2011). Phosphatases: providing safe passage through mitotic exit. *Nat. Rev. Mol. Cell Biol.* **12**, 469-482.
Yeong, F. M., Lim, H. H., Padmashree, C. G. and Surana, U. (2000). Exit from mitosis in budding yeast: biphasic inactivation of the Cdc28-Clb2 mitotic kinase and the role of Cdc20. *Mol. Cell* **5**, 501-511.

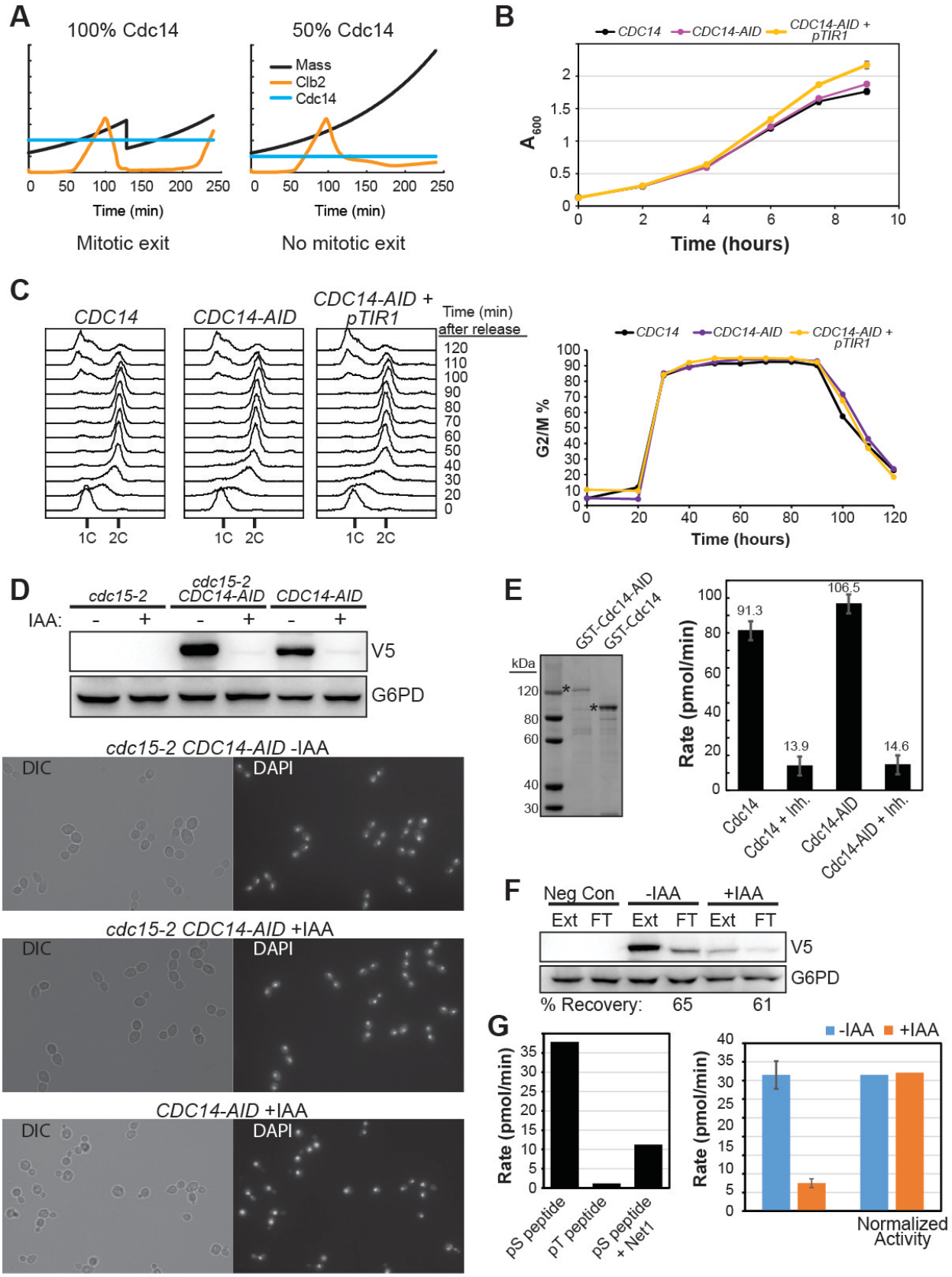

Figure S1. Additional characterization of *CDC14-AID* strain and Cdc14-AID protein. A. In this model (Drapkin et al., 2009), Cdc14 directly reduces the total level of Cdk activity according to the equation Clb2 - (k)*Cdc14 - KEZ = 0, where (k) is the Cdc14 'strength factor' to parameterize Cdc14 activity relative to Clb2-Cdk and KEZ is the threshold for mitotic exit. MATLAB was used to predict the impact of reducing Cdc14 concentration on mitotic exit. Left, starting parameters defined in (Drapkin et al., 2009). Right, Cdc14 reduced to 50% of the starting level was sufficient to block mitotic exit and cell division. Cells were allowed to cycle over 250 minutes. Black, cell mass; Orange, Clb2 level; Cyan, total Cdc14. **B.** Growth rates of liquid YPD cultures of parental W303 and the engineered *CDC14-AID* strain before and after integration of the *pTIR1* plasmid were compared. Cultures were grown to mid-log phase and then back-diluted to OD_{600} = 0.1 in fresh medium to initiate the experiment. Data are the average of 3 trials with standard deviation error bars (too small to see on most data points). A_{600} is absorbance at 600 nm. **C.** Liquid cultures of the same strains from panel B were arrested in G1 with 5 µg/ml alpha factor and then released into fresh YPD medium lacking alpha factor. Cells were harvested at the indicated time points and DNA content analyzed by flow cytometry. Alpha factor was added back at 75 minutes to arrest cells in the following G1 so that kinetics of a single cycle could be monitored. Quantitation of the 2C DNA content in the profiles on the left was performed using FCS Express (De Novo Software) and is plotted on the right. **D.** Strains *cdc15-2* (not shown), *cdc15-2 CDC14-AID,* and *CDC14-AID* were grown in liquid culture to early log phase at room temperature. Cultures were split, 250 µM IAA was added to half, and after a 15 min incubation cultures were shifted to 37 °C for 2.5 hours. Cells were fixed in 70% ethanol overnight at 4 °C, stained briefly with 1 µg/ml DAPI, washed extensively with PBS and imaged by DIC and epifluorescence microscopy. Additional cells were processed for anti-V5 immunoblotting (top) to verify Cdc14-AID depletion. G6PD is a loading control. Arrest morphology of *cdc15-2* and *cdc15-2 CDC14-AID* was similar (large-budded cells with segregated DNA masses). **E.** Left, Coomassie blue-stained SDS-PAGE of recombinant GST-Cdc14-AID and GST-Cdc14 (indicated by *) preparations from *E. coli*. ImageLab software (Bio-Rad) was used to determine protein concentrations based on band intensities. Right, specific activities of the two preparations (90 nM each) towards 25 mM *p*-nitrophenyl phosphate are compared. “Inh.” - sodium orthovanadate, an inhibitor of the protein tyrosine phosphatase superfamily, was used at 500 µM to demonstrate that activity in each prep is from Cdc14. Data are the average of 3 trials with standard deviation error bars. **F.** Anti-V5 antibody resin was used to isolate Cdc14-AID protein from soluble extracts of *CDC14-AID* cells either untreated or treated with 500 µM IAA for 30 min. “Neg Con” is the untagged parental W303 strain.

Comparing the starting extract (Ext) to the resin flow-through (FT) revealed nearly identical recovery efficiencies of >60% for +/- IAA. This shorter IAA treatment resulted in 80% Cdc14-AID depletion and was used to ensure recovery of measurable phosphatase activity. **G.** Left panel, phosphatase activity associated with the –IAA anti-V5 resin from panel F towards 200 μM peptide substrate MI(pS)PSKKRTI (pS = phosphoserine) was inhibited by addition of 10 μg recombinant GST-Net1(1-600) and was eliminated when using 200 μM peptide variant MI(pT)PSKKRTI containing phosphothreonine (pT) in place of phosphoserine. Right panel, relative activities of equivalent fractions of anti-V5 resins from –IAA and +IAA preparations towards the MI(pS)PSKKRTI peptide substrate are shown in bars at left (averages of 3 reactions with standard deviation error bars). Immunoblotting and quantitation of the V5 epitope signal associated with the resin in each reaction (not shown) allowed normalization for the differences in Cdc14-AID abundance in the –IAA and +IAA preps, shown in the “Normalized Activity” bars at right.

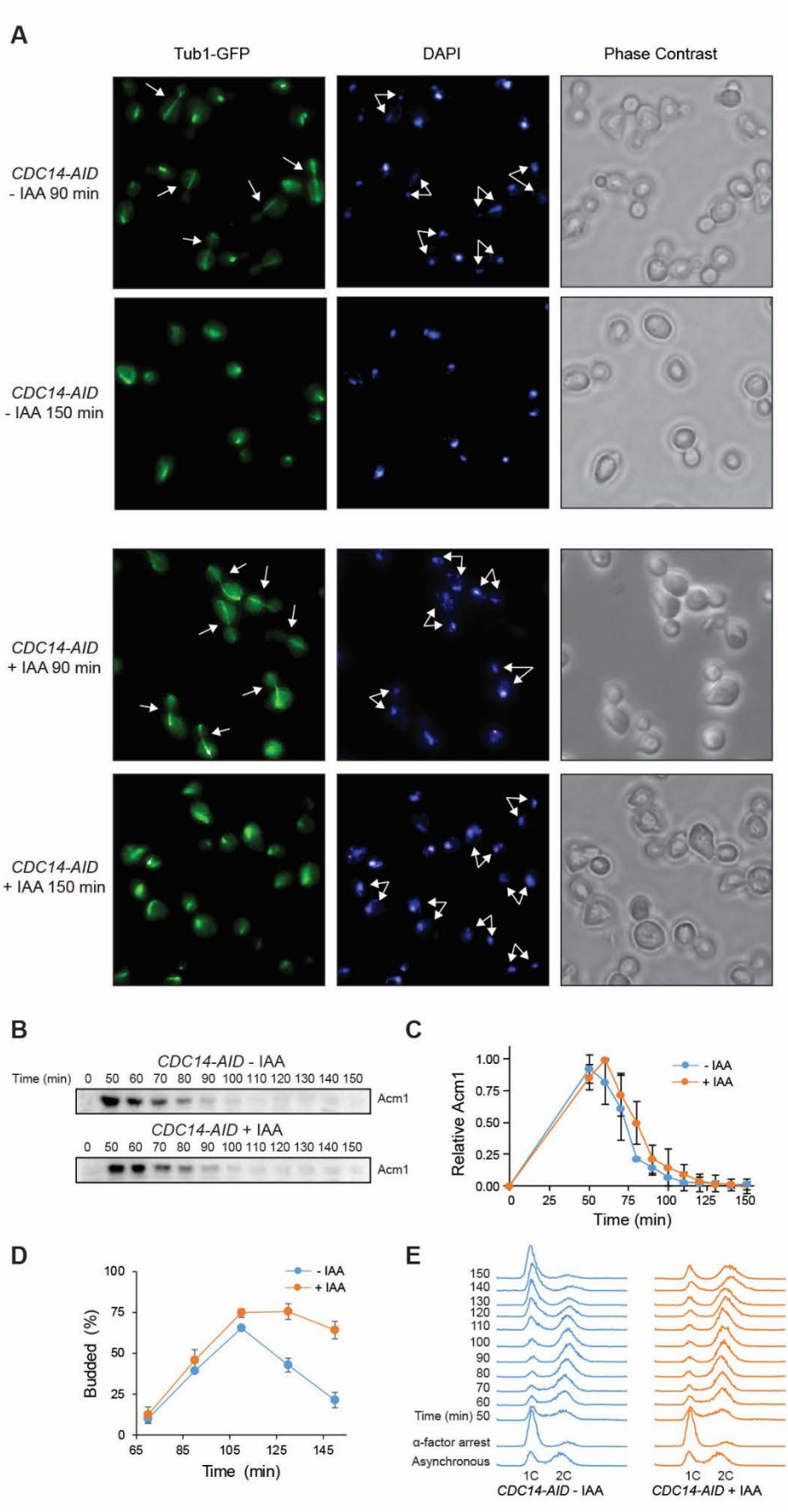

Figure S2. Cdc14-depleted cells have normal spindle disassembly and chromosome segregation, but defective or delayed cell separation. A. Spindle assembly (Tub1-GFP) and chromosome segregation (DAPI) were monitored by fluorescence microscopy. Overall cell morphology and bud status were monitored by phase contrast microscopy. Representative images from 90 minutes and 150 minutes after release are shown highlighting intact, elongating anaphase spindles, defined as continuous linear GFP signal stretching between mother and daughter cells (arrows in Tub1-GFP panels) and segregated DNA (arrows in DAPI panels). Spindles completely disassemble as cells complete mitotic exit in the presence of IAA, despite the genetic requirement for *CDC14* at this step. However, mother and daughter cells do not separate as efficiently in the IAA-treated cultures as evidenced by the persistent large-budded cells at the 150 min time point. **B.** The Cdk phosphorylation-dependent stability of Acm1 (52) was monitored by anti-Acm1 immunoblotting. Dephosphorylation of Cdk sites on Acm1 is required for its degradation during mitotic exit and therefore Acm1 stability **C.** Acm1 levels were quantified from the digital images in panel C and normalized to peak intensity. **D.** The fraction of budded *CDC14-AID* cells with or without 250 μM IAA treatment was determined by phase contrast microscopy and plotted as a function of time after synchronous release from G1 arrest. Data are averages of three independent experiments with standard deviations. **E.** DNA content of the same cultures was monitored by flow cytometry. The IAA-treated cells have a delayed return to 1C DNA content. The persistent budded morphology and 2C DNA content indicated cells are not separating efficiently, despite completing mitotic exit normally.

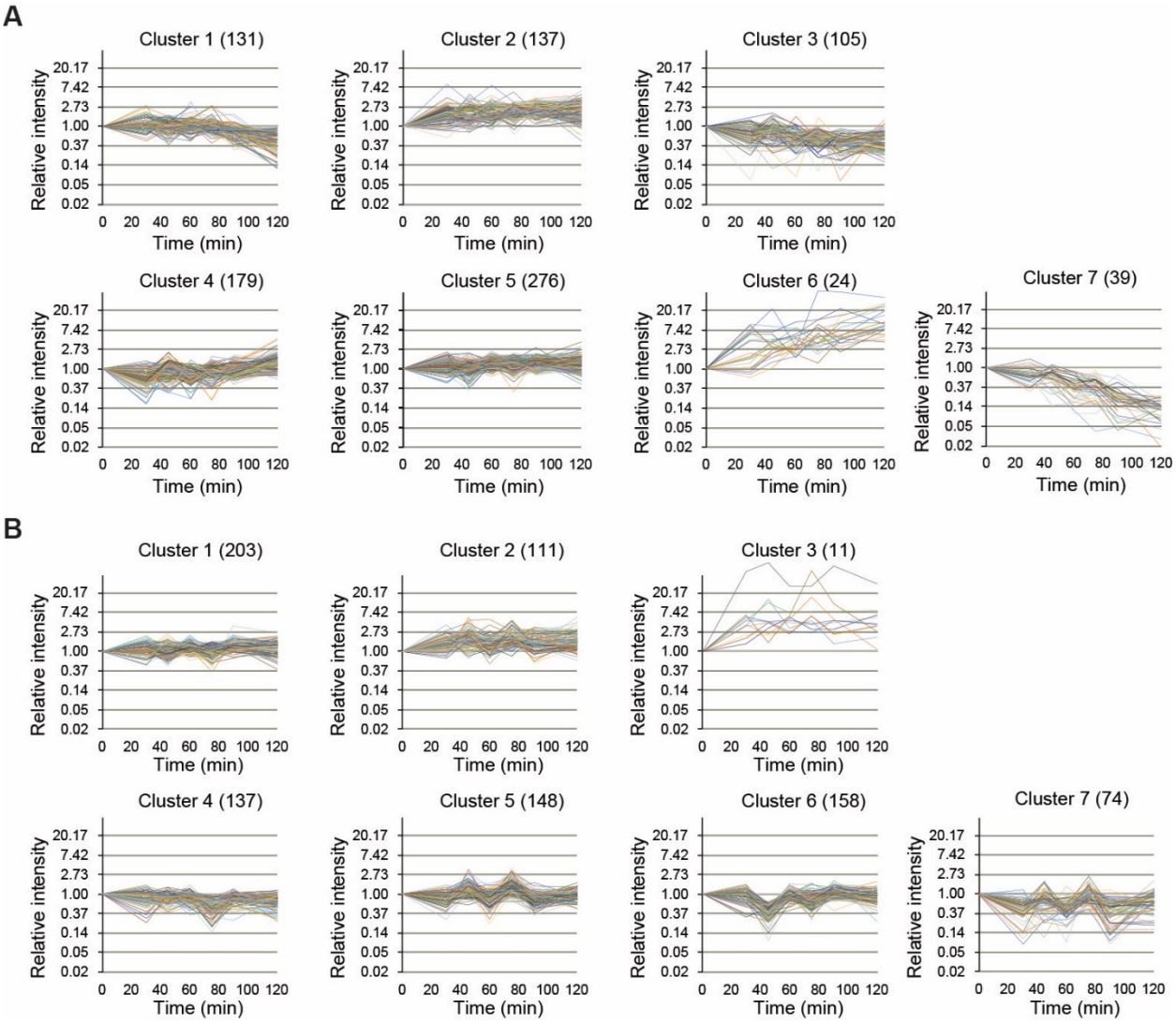

Figure S3. Soft clustering analysis of SWATH phosphopeptide profiles. A. Temporal phosphopeptide intensity profiles from pGAL1-CDC14-3MYC were subjected to soft clustering (number per cluster is indicated; 51 were unclustered). Clusters 3 and 7 contained decaying peptide signals and were further processed and evaluated as possible Cdc14 substrates. Clusters 1, 2, 4, and 5 contained stable peptide signals. Cluster 6 contained phosphopeptides with increasing signals and included peptides from Sic1, whose expression is induced by Cdc14, and proteins like Gal1 and Gal7 involved in the response to galactose. **B.** Temporal phosphopeptide intensity profiles from the empty vector control were subjected to soft clustering (number per cluster is indicated; 100 were unclustered). All clusters contained stable peptide signals with the exception of Cluster 3, which contained peptides with increasing signal.

Table S1. Quantitative phosphoproteomic analysis of in vivo Cdc14 specificity by SWATH-MS. The page titled "Extracted Profiles" lists all quantified phosphopeptides. To generate this collection of high confidence phosphopeptides, the following processing protocol was used. First, all non-phospho peptides were removed, as were phosphopeptides with poor signal quality indicated by an average extraction FDR > 90% across all samples. The remaining SWATH signals were then quantile normalized as described (Callister et al., 2006) in Microsoft Excel. Briefly, the raw intensities for each peptide were arranged in columns based on sample and time point, assigned an index value, and sorted from least to greatest intensity. After sorting, the mean abundance for each row was substituted for each raw intensity value in that row and then the original order was restored using the index values. These normalized intensities for each peptide were then averaged across time points. The resulting average intensities were then further normalized to the intensity at time 0, natural log-transformed, and plotted to generate decay profiles that could be fit by linear regression (assuming that typical dephosphorylation kinetics would follow an exponential decay). The linear equations were used to calculate half-life values for each peptide (the time at which phosphopeptide signal reached 50% of its initial value). Phosphopeptide profiles were then subjected to a final filtering regimen to prepare a list of high confidence phosphorylation sites. To obtain probability-based scores for phosphosite mapping confidence, ProteinPilot-processed spectra were exported as .mgf files and searched using Mascot v 2.5.1 MS/MS ions search (Matrix Science, Boston, MA) with the following parameters: trypsin, fixed carbamidomethyl (C), variable phospho (ST) and oxidation (M), peptide mass tolerance +/- 20 ppm, fragment mass tolerance +/- 0.6 Da, and up to 2 missed cleavages. We removed all multiply phosphorylated peptides (because it was too difficult to reliably distinguish which of the sites were dephosphorylated), and phosphopeptides with Mascot scores below a 1% FDR cutoff and/or PTM site analysis confidence < 75%, and peptides with duplicate phosphorylation sites that resulted, for example, from missed cleavages. In both the "Extracted Profiles" and "Rapidly Dephosphorylated" lists, the columns are defined as follows. A, an index number for sorting. B, Swiss Protein data bank accession number. C, protein name from the Saccharomyces cerevisiae genome database. D, the phosphorylated residue number within the protein. E, proteins previously identified as S. cerevisiae Cdk substrates in large-scale studies (A = Ubersax et al. Nature 2003, 425: 859-64 (p-value > 2.0) and B = Holt et al. Science 2009, 325: 1882-6 (only the 547 high confidence substrates included). F, the site confidence obtained from Mascot. G, the sequence surrounding the phosphorylated site. H, the site class where pS is phosphoserine and pT is phosphothreonine. I, the peptide sequence identified in the spectral library. J, observed m/z for the peptide. K, observed charge state of the peptide. L, peptide's HPLC retention time used for SWATH extraction. M, the average false detection rate (FDR) of SWATH extraction. N-T, time points in minutes with the LN-scaled relative abundance values. U, the number of missing values from the peptide profiles. V-X, measures of linear regression for rapidly dephosphorylated clusters 3 and 7. Y, The assigned cluster from fuzzy-c means clustering. Z, the degree of fit within a cluster. AA-AG, time points in minutes with the LN-scaled relative abundance values. AH, the number of missing values from the peptide profiles. AI-AK, measures of linear regression (including the slope, the fit, and the estimated 1/2 life) for rapidly dephosphorylated clusters 3 and 7. AL, The assigned cluster from fuzzy-c means clustering. AM, the degree of fit within a cluster.

Click here to Download Table S1

Table S2. GO term enrichment among rapidly dephosphorylated proteins.

GO Term	Accession	p-value	Genes
Regulation of exit from mitosis	0007096	1.74E-04	MOB1, CDC14, NET1, CLA4
Cell division	0051301	2.77E-04	IQG1, MOB1, SMC4, POG1, SSD1, CDC14, NET1
Cell cycle	0007049	0.004	IQG1, MOB1, SMC4, POG1, SSD1, CDC14, NET1
Regulation of transcription involved in G1/S transition of mitotic cell cycle	0000083	0.0063	HOS3, SWI4, SWI5
Mitotic nuclear division	0007067	0.011	SMC4, POG1, SSD1, CDC14, POG1
Nucleolus organization	0007000	0.0134	TOF2, NET1
Negative regulation of septation initiation signaling	0031030	0.0134	TOF2, NET1
Endoplasmid reticulum polarization	0061163	0.02	SHS1, YMR124W
rDNA condensation	0070550	0.0589	TOF2, SMC4

Table S3. Yeast strains used.

Strain	Genotype	Source
W303	MATa *leu2-3,112 trp1-1 can1-100 ura3-1 ade2-1 his3-11,15*	
YKA890	W303 MATa *CDC14-V5-AID:KanMX*	This study
YKA892	W303 MATa *CDC14-V5-AID:KanMX leu2::P_{ADH1}-TIR1::LEU2*	This study
YKA1013	W303 MATa *ura3::P_{HIS3}-GFP-TUB1:URA3 his3::P_{CDH1}-3FLAG-CDH1:HIS3*	This study
YKA1014	W303 MATa *CDC14-V5-AID:KanMX leu2::P_{ADH1}-TIR1::LEU2 ura3::P_{HIS3}-GFP-TUB1:URA3 his3::P_{CDH1}-3FLAG-CDH1:HIS3*	This study
YKA1034	W303 MATa *CDC14-V5-AID:KanMX leu2::P_{ADH1}-TIR1::LEU2 ura3::P_{HIS3}-GFP-TUB1:URA3 his3::P_{CDH1}-3FLAG-CDH1:HIS3 cdc15-2*	This study
BY4741	MATa *his3Δ1 leu2Δ0 met15Δ0 ura3Δ0*	
ASK1-TAP	BY4741 *ASK1-TAP:HIS3*	Dharmacon Inc, Lafayette, CO
HCY114	W303 *cdc14-1*	(Hall et al., 2008)
DLY3034	W303 MATα *cdc15-2*	Daniel Lew, Duke University

Table S4. Yeast plasmid constructs used.

Plasmid Name	Origin[1]	Marker[1]	Promoter	Expressed Protein	Source
pESCLeu	2 micron	*LEU2*	*GAL1*	-	Agilent Technologies, Santa Clara, CA
pESCLeu-*CDC14-3MYC*	2 micron	*LEU2*	*GAL1*	Cdc14-3Myc	This study
pRS306-*TUB1*	Integrating	*URA3*	*HIS3*	GFP-Tub1	(Martinez et al., 2012)
pAR1103	Integrating	*LEU2*	*ADH1*	Tir1[3]	Adam Rudner, University of Ottawa
pAR1070[2]	-	KanMX	-	-	Adam Rudner, University of Ottawa

[1]Origin and Marker are for propagation and selection in budding yeast cells.

[2]pAR1070 was used as a template to amplify the V5 epitope/AID tag with the KanMX marker for integration at the 3' end of the CDC14 gene.

[3]From the Oryza sativa TIR1 gene.